

Geophysical Research Letters®

RESEARCH LETTER

10.1029/2021GL097382

Key Points:

- We observe foreshocks dynamic characteristics before the 2009, Mw 6.1 L'Aquila earthquake in central Italy
- Deviations of radiated energy over seismic moment from a reference model highlight the preparatory phase of the main event
- Foreshocks are characterized by a progressive increase in slip per unit stress, in agreement with diffusion of highly pressurized fluids

Supporting Information:

Supporting Information may be found in the online version of this article.

Correspondence to:

M. Picozzi,
matteo.picozzi@unina.it

Citation:

Picozzi, M., Spallarossa, D., Iaccarino, A. G., & Bindi, D. (2022). Temporal evolution of radiated energy to seismic moment scaling during the preparatory phase of the Mw 6.1, 2009 L'Aquila earthquake (Italy). *Geophysical Research Letters*, 49, e2021GL097382. <https://doi.org/10.1029/2021GL097382>

Received 7 DEC 2021

Accepted 28 MAR 2022

Author Contributions:

Conceptualization: M. Picozzi, D. Spallarossa, D. Bindi
Data curation: D. Spallarossa
Formal analysis: M. Picozzi, D. Spallarossa
Investigation: M. Picozzi, A. G. Iaccarino, D. Bindi
Methodology: M. Picozzi, D. Spallarossa, A. G. Iaccarino, D. Bindi
Resources: M. Picozzi, D. Spallarossa
Software: M. Picozzi, D. Spallarossa

© 2022. The Authors.

This is an open access article under the terms of the Creative Commons Attribution-NonCommercial-NoDerivs License, which permits use and distribution in any medium, provided the original work is properly cited, the use is non-commercial and no modifications or adaptations are made.

Temporal Evolution of Radiated Energy to Seismic Moment Scaling During the Preparatory Phase of the Mw 6.1, 2009 L'Aquila Earthquake (Italy)

M. Picozzi¹ , D. Spallarossa^{2,3}, A. G. Iaccarino¹ , and D. Bindi⁴ 

¹University of Naples Federico II, Naples, Italy, ²DISTAV, University of Genoa, Genoa, Italy, ³Istituto Nazionale di Geofisica e Vulcanologia (INGV), Milan, Italy, ⁴GFZ German Research Centre for Geosciences, Helmholtz Centre Potsdam, Potsdam, Germany

Abstract We investigate the preparatory phase of the 2009, Mw 6.1 L'Aquila earthquake in central Italy by analyzing the temporal evolution and spatial distribution of the seismic moment, M_0 , to radiated energy, E_S . Our approach focuses on monitoring the deviations of the scaling between M_0 and E_S with respect to a model calibrated for the background seismicity. The temporal evolution of these deviations, defined as Energy Index (EI), identifies the onset of the activation phase 1 week before the mainshock. We show that foreshocks are characterized by a progressive increase in slip per unit stress, in agreement with the diffusion of highly pressurized fluids before the L'Aquila earthquake proposed by previous studies. Our results suggest that the largest events occur where energy index (EI) is highest, in agreement with the existing link between energy index (EI) and the mean loading stress.

Plain Language Summary Understanding how the machine generating large earthquakes works is one of the fundamental challenging scientific questions. Pioneering studies have shown that large magnitude earthquakes are sometimes anticipated by foreshocks and slip instabilities. Until now, retrospective analyses of foreshocks during the preparatory phase of large earthquakes have focused mainly on their distribution in space, time and magnitude. In this study, we show that also the dynamic properties of the rupture process associated to foreshocks evolve both in time and space. Our results indicate that the temporal evolution of radiated energy and size of small magnitude earthquakes provide useful information to identify the begin of the final activation phase of the 2009 Mw 6.1 L'Aquila, Italy, earthquake, in agreement with seismicity rate information. Our study suggests that, for the investigated case, foreshocks had dynamic characteristics distinct from those of normal rate (background) seismicity. Thus, it can contribute with new evidence to the open debate whether foreshocks are different phenomena from background seismicity.

1. Introduction

The impact of large earthquakes is not only important in terms of casualties and damages in epicentral areas, but also for the domino effects on our globalized society that can lead to losses of billions of euros. Although enormous efforts have been made in the last century to strengthen seismic monitoring, forecasting of large earthquakes remains an unresolved fundamental scientific question.

Retrospective studies on megathrust earthquakes (e.g., Schurr et al., 2014; Socquet et al., 2017) have shown that the complex multi-scale generation process of large earthquakes might have different dominant features (e.g., foreshocks or slow slip events and creep phenomena identifiable by geodetic measurements) depending on the tectonic environment. As a result of scientific developments in infrastructures and data-mining strategies, systematic patterns in seismicity and crustal deformation preceding large earthquakes have started to emerge (Bouchon et al., 2013; Kato et al., 2012; Malin et al., 2018; Socquet et al., 2017; Yoon et al., 2019), showing that micro- and small-magnitude events before large earthquakes can highlight temporal and spatial peculiar patterns in their evolution.

Kato and Ben-Zion (2020) suggested for the generation of large earthquakes the progressive localization of shear deformation around a rupture zone that evolves into a final rapid loading (i.e., generating foreshocks) of a volume localized nearby the hypocenter of the major dynamic rupture. Such kind of process may be universal, being similar patterns of damage evolution across a fault zone found by studying acoustic emissions during triaxial

Writing – original draft: M. Picozzi,
D. Bindi

Writing – review & editing: D.
Spallarossa, A. G. Iaccarino, D. Bindi

tests on rock samples (Dresen et al., 2020). While slow slip events and foreshocks occurrence are quite common in subduction zone faults, so far, they are rarely observed in other tectonic contexts.

Although not very large in magnitude, the 6th April 2009 Mw 6.1 L'Aquila, Italy, earthquake, which caused 308 casualties and damage over a large area, is very well known by the scientific community for the trial of seismologists (Abbott & Nosengo, 2014), which generated a new awareness of the need to improve the communication of natural risks.

The 2009 Mw 6.1 L'Aquila, Italy, earthquake, occurred on a continental normal fault, known as Paganica fault (Boncio et al., 2010) and it was preceded by foreshocks clustered near the nucleation area of the mainshock (Chiaraluce et al., 2011; Malagnini et al., 2012; Terakawa et al., 2010; Valoroso et al., 2013), with the latter associated with a slow-slip event identified by analysis of geodetic data (Borghi et al., 2016). Previous studies on the preparatory phase of the 2009 L'Aquila earthquake have shown: foreshocks migration at a rate of ~0.5 km/day toward the nucleation point of the main shock (Sgan et al., 2014); b-value changes (De Gori et al., 2012); changes in the elastic properties of the medium (Di Luccio et al., 2010; Lucente et al., 2010); different source properties between foreshocks and aftershocks (Calderoni et al., 2019).

In this work, we study the seismicity around the 2009 Mw 6.1 L'Aquila earthquake (Figure 1) considering a catalog of 6,188 earthquakes with magnitude between Mw 1.8 and Mw 6.1 that occurred in the period between the begin of the 2005 to the end of 2009.

We show that seismic moment (M_0) and radiated seismic energy (E_s) estimates of small magnitude earthquakes can highlight new information on the dynamic of ruptures occurring before the mainshock, which allows us to gain a new perspective on the study of the preparatory phase of the Mw 6.1, 2009 L'Aquila earthquake.

In the wake of works showing that E_s and M_0 together allows to look at the complexity of a seismic source, with M_0 being a static measure of the earthquake size and E_s being related to the kinematics and dynamics of the rupture (Bindi et al., 2018, 2019; Picozzi et al., 2017, 2018; Picozzi, Bindi, & Spallarossa, 2019; Picozzi, Bindi, Zollo, 2019), recently, Spallarossa et al. (2021) implemented an innovative service for the Rapid Assessment of Seismic Moment and Radiated Energy in Central Italy (RAMONES).

Here, we rely on E_s and M_0 estimates for the 2009 L'Aquila earthquake sequence derived following the procedure implemented within the RAMONES service and on earthquake locations obtained using the approach by Scafidi et al. (2019). Our study focuses on the spatio-temporal evolution of the linear scaling between the logarithm of E_s and M_0 . Our main objective is to verify whether foreshocks are characterized by dynamic characteristics distinct from those of normal rate (background) events, as found by Chen and Shearer (2013) in Southern California and by Calderoni et al. (2019) on a restricted data set for the 2009 L'Aquila earthquake consisting of 11 foreshocks and 12 aftershocks. Our study, thus, aims on the one hand to improve our understanding of the physical processes that lead to the 2009 L'Aquila earthquake sequence; on the other hand, we aim at providing new evidence to the open debate whether foreshocks are different phenomena from background seismicity. Indeed, the identification of peculiar features of foreshocks and their patterns of occurrence could foster new developments in forecasting large earthquakes.

2. Data

RAMONES extracts and analyses segments from continuous data streams stored in the ORFEUS-EIDA, IRIS and DPC repositories (Spallarossa et al., 2021). In this study, we consider the period from the 1st January 2005 to the 31st December 2009. Following the automatic procedure described in Spallarossa et al. (2014) and Scafidi et al. (2019), P and S onsets are detected, event locations and local magnitudes are estimated, and features related to M_0 and E_s are extracted from recordings. Uncertainties in event location are mostly within 1 km both horizontally and vertically (Figure S1 in Supporting Information S1). Using empirical attenuation models calibrated for a wide region of the central Apennines (Italy) by Spallarossa et al. (2021) (i.e., within a region bounded by 40.0°N and 44.5°N in latitude and 10.50°E and 16.50°E in longitude), M_0 and E_s are estimated for 6,188 earthquakes in the magnitude range from Mw 1.7 to Mw 6.1 and depths range from 1 to 30 km. The number of stations per event on which M_0 and E_s estimates are obtained ranges mostly between 10 and 40 (Figure 1 and Figure S2 in Supporting Information S1). For the sake of simplicity, we refer to Spallarossa et al. (2021) for more details on the procedure for estimating M_0 and E_s and for a validation of the results.

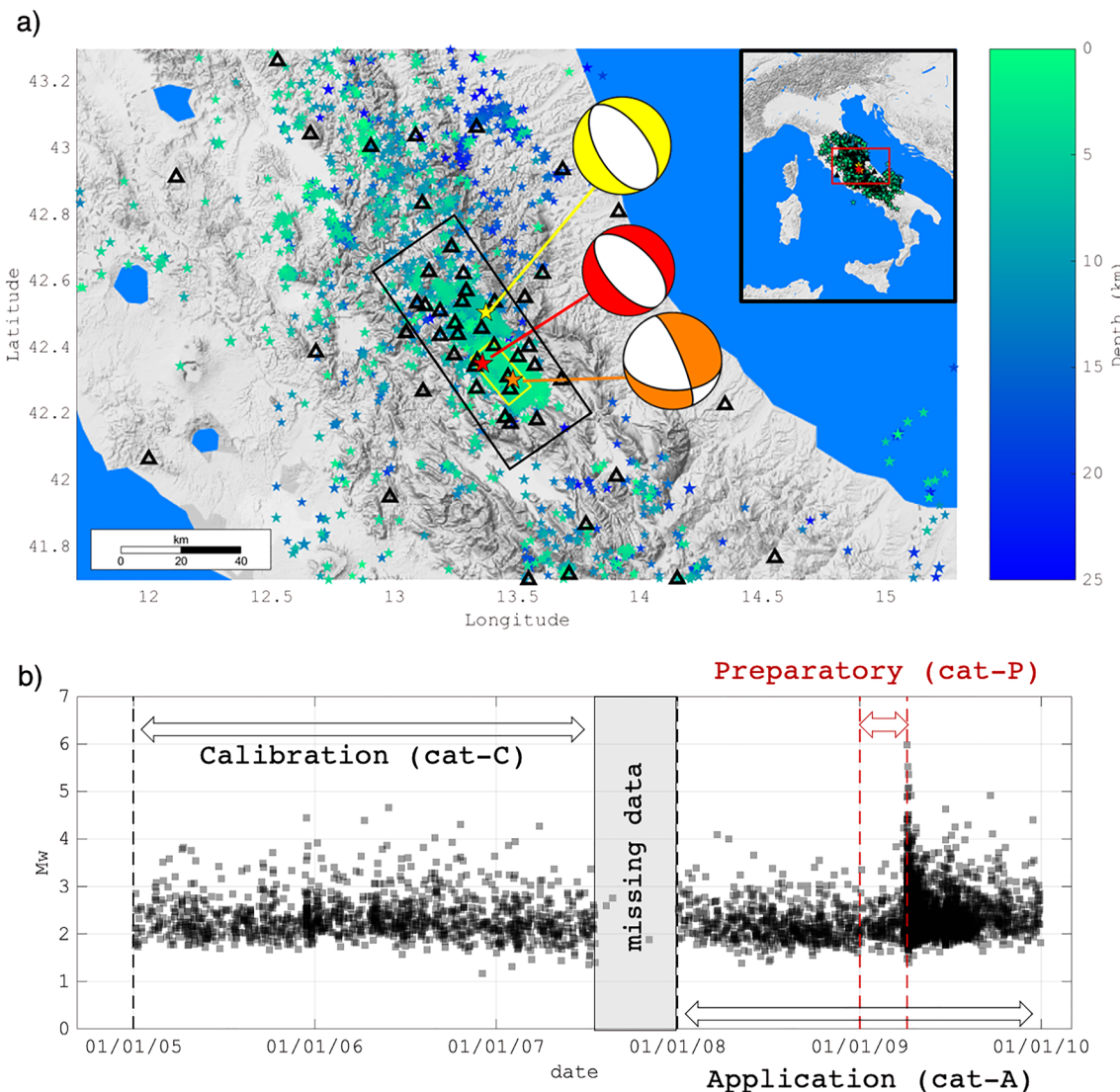


Figure 1. (a) Overview map: seismic stations (black triangles), epicenter of seismic events (stars colored per hypocentral depth), Mw 6.1 L'Aquila epicenter (red star), Mw 5.2 aftershock (orange star), Mw 5.4 Campotosto earthquake (yellow star), focal mechanism for the three main events of the seismic sequence are shown (i.e., the 06-04-2009 01:32:40 (UTC) event, <http://cnt.rm.ingv.it/event/1895389> in red; the 07-04-2009 17:47:37 (UTC) event, <http://cnt.rm.ingv.it/event/1908319> in yellow; the 09-04-2009 00:52:59 (UTC) event, <http://cnt.rm.ingv.it/event/1916789> in orange). (b) Distribution of Mw in time. Limits of the calibration period (dashed black line) and limits of the preparatory phase (dashed red line).

Bindi et al. (2020) developed a numerical study to evaluate the resolution limits of source parameters for data recorded in the same region considered in this study. They found that reliable source parameters (M_0 and E_s) can be retrieved for earthquakes above Mw 1.8, without strong bias due to unaccounted attenuation effects. The same magnitude threshold was adopted by Mignan (2012) to study the seismicity rate observed before the 2009 Mw 6.1 L'Aquila earthquake. Therefore, in the following, we set the minimum magnitude of the considered events equal to Mw 1.8 for our analysis. As shown in Figure 1b, for the period from 1st September 2007 to 31st December 2007 the data cannot be retrieved through any of the services mentioned above (personal communication INGV Rome).

We split the data set into two parts. Data from 1st January 2005 to 1st September 2007 (i.e., 1,237 earthquakes; hereinafter, cat-C) are used for the calibration of a reference scaling model between the base-10 logarithm of the estimated seismic moment, $\log(M_0)$, and radiated energy, $\log(E_s)$. Cat-C period sees the absence of large earthquakes. Thus, we can reasonably assume that it gives us a picture in terms of radiated energy versus seismic moment, relevant for background seismicity.

Data from 1st January 2008 to the 31st December 2009 (i.e., 4,951 earthquakes; hereinafter, cat-A) are then used to study the deviations of $\log(E_S)$ and $\log(M_0)$ estimates from the reference scaling model. Within cat-A, particular attention is paid to a sub-dataset relevant for the preparatory phase (Figure 1b), which includes data from 1st January 2009 to the 9th September 2009 (i.e., 774 earthquakes; hereinafter, cat-P).

3. Energy-to-Moment Scaling and Energy Index

We use cat-C data to calibrate the following scaling model of seismic radiated energy versus seismic moment

$$\log(E_S) = a \log(M_0) + b \quad (1)$$

where a is equal to 1.31 (± 0.01) and b is equal to -9.72 (± 0.12), with residuals standard deviation equal to 0.22 and R^2 equal to 0.89 (Figure 2a).

Brown and Hudyma (2017) proposed to use the differences between experimental E_S estimates and theoretical E_S values derived from a scaling model such as Equation 1, where the input is the seismic moment M_0 from recorded earthquakes, as an indicator of the stress around mining sites. Similarly, we define the Energy Index (EI) as the difference between the observed E_S and the values associated with the median E_S -to- M_0 scaling model (Equation 1; hereinafter referred to as the reference model, E_{S-R})

$$EI = \log(E_{S-obs}) - \log(E_{S-R}) = \log(E_{S-obs}) - [a \log(M_{0-obs}) + b] \quad (2)$$

Figure (2a) shows the $\log(E_S)$ versus $\log(M_0)$ scaling for both cat-C (green) and cat-A (black) data, and it exemplifies the main concepts associated to energy index (EI). Whenever energy index (EI) is positive, the considered event has radiated more energy per unit-slip and unit-area (i.e., M_0) than expected by the model describing the behavior of background seismicity. Conversely, negative EI are associated with events characterized by an excess of slip compared to the expected value considering the radiated energy, or same slip but larger rupture area and lower stress drop.

Figure (2b) shows the distribution of EI for cat-C and cat-P data (similar plots for cat-A before and after the 2009 Mw 6.1 L'Aquila earthquake are shown in Figure S3 in Supporting Information S1), while Figure (2c) shows the temporal evolution of EI for the whole data set, with uncertainty on EI derived by combining those from experimental E_S and model (1). Figure (2c) shows sliding average of EI (+/- the standard deviation) computed on 90 events moving windows for magnitude in the range Mw 1.8–3.5 and depth 6–15 km. The exclusion of events with $Mw > 3.5$ (i.e., 135 in total) is done to avoid that larger magnitude events, possibly characterized by higher E_S per M_0 than smaller ones (see Kanamori & Heaton, 2000), inflate the temporal evolution of EI. The selected depths correspond to the interval where the foreshock sequence occurred, with a progressive migration of events toward the base of the normal fault where the mainshock nucleated (at about 9 km of depth, Sugan et al., 2014). The absence of both anomalous values and trends with time in the average EI values suggests that EI is stationary in the cat-C period. On the contrary, we observe for cat-A a strong decrease in EI at the time of the mainshock and for the subsequent aftershocks, followed by a progressive recover to values compatible with the reference period.

Before moving into a detailed analysis of the temporal and spatial EI variability, we suggest a possible physical meaning of this parameter. Following Wyss and Brune (1968), the radiated energy to seismic moment ratio (i.e., the scaled energy) corresponds to the apparent stress, τ_a , over the seismic rigidity module, μ (i.e., $E_S/M_0 = \tau_a/\mu$).

Therefore, considering the following relation

$$\log(E_S) = \log(M_0) + \log(\tau_a) - \log(\mu), \quad (3)$$

we can see the EI in Equation 2 as

$$EI = [\log(M_{0-obs}) + \log(\tau_a) - \log(\mu)] - [a \log(M_{0-obs}) + b] \quad (4)$$

As the logarithm of the seismic moment of considered events varies from 11.8 to 13.85 Nm, the term $\log(M_{0-obs}) - a \log(M_{0-obs}) = -0.31 \cdot \log(M_{0-obs})$ varies between -4.3 and -3.7 .

The S-wave velocities between 4.5 and 14.5 km of depth range between 3.15 and 3.43 km/s (Hermann et al., 2011), whereas the density is between 2.6 and 2.7 g/cm³. Hence, we can assume μ ranging between $26 \cdot 10^9$

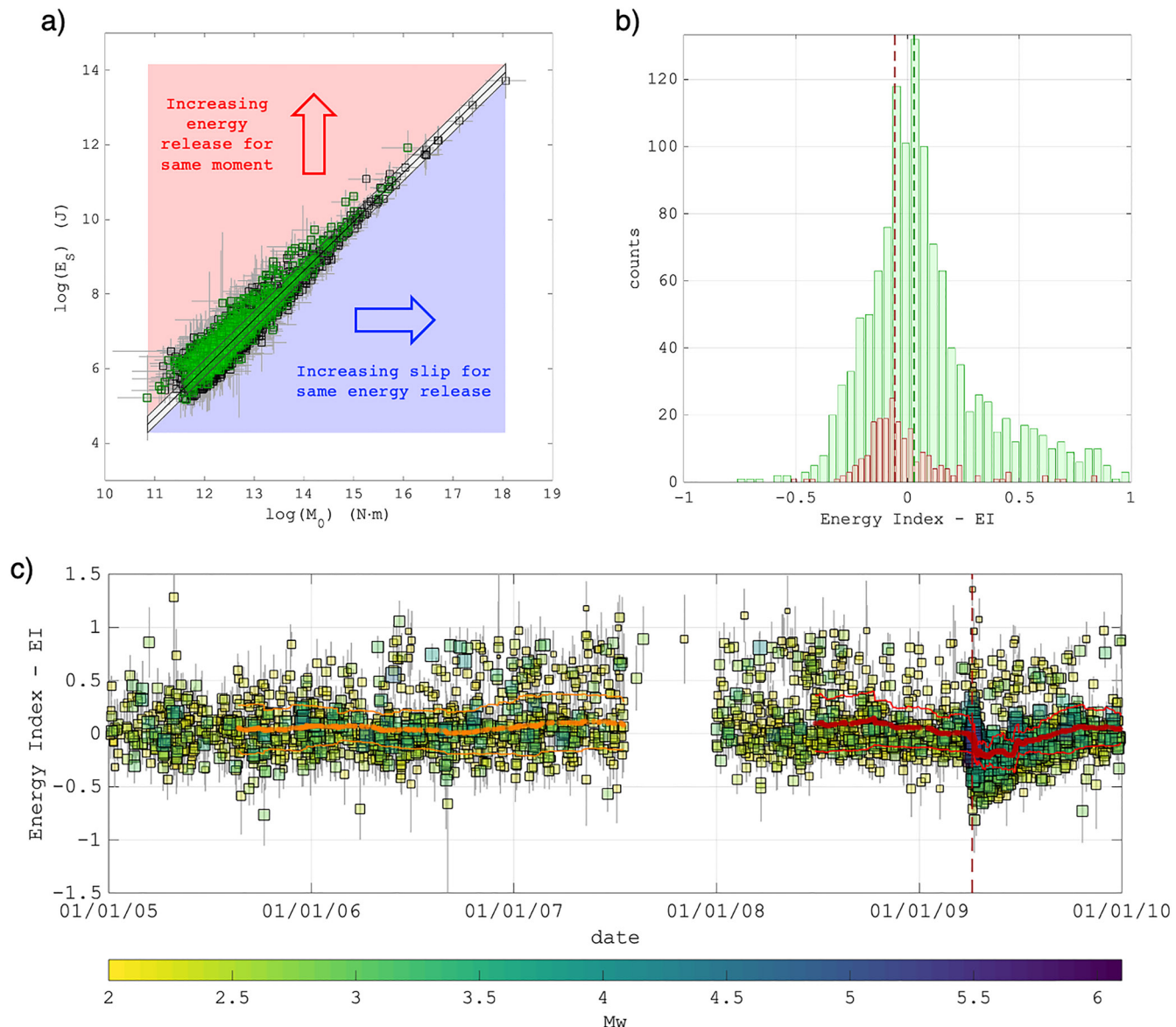


Figure 2. (a) Scaling of the logarithm of radiated energy E_s with logarithm of seismic moment M_0 and ± 1 standard deviation for the estimated parameters (horizontal and vertical black lines, respectively) for both cat-C (green) and cat-A (black) data, the best-fit scaling model, Equation 1 (mean ± 1 standard deviation are shown as black lines). (b) Histogram showing the distribution of the Energy Index (EI) for cat-C (green) and cat-P (red) with median values highlighted by dashed vertical lines. (c) Temporal evolution of EI with associated their standard errors (square colored and with varying size per magnitude), 90 events moving average of EI for events belonging to the calibration period (orange) and for the preparatory phase and after L'Aquila earthquake (red). The time of occurrence for the L'Aquila earthquake (red dashed line) is also plotted. Mean EI is not shown for periods for which the window has less than 90 events.

and $33 \cdot 10^9$ Pa, leading the term $-\log(\mu)$ to be between -10.4 and -10.5 . Therefore, the combination of terms b and $-\log(\mu)$ in Equation 4 varies between -0.8 and -0.7 .

Combining all aforesaid numerical terms, Equation 4 can be seen as

$$EI = \log(\tau_a) - 4.75 (+/- 0.35) \quad (5)$$

Equation 5 suggests a direct proportionality between EI and τ_a . The scaling between EI and $\log(\tau_a)$, with the latter being derived using μ equal to $33 \cdot 10^9$ Pa as in Calderoni et al. (2019), is shown in Figure S4 in Supporting Information S1 and compared to Equation 5.

For the interpretation of our results, it is useful also to consider the definition of apparent stress provided by McGarr (1999), that is $\tau_a = \eta \bar{\tau}$, where η is the seismic efficiency and $\bar{\tau}$ is the mean loading stress during an event. Therefore, at least as first approximation,

$$EI \propto \log_{10}(\tau_a) \approx \log_{10}(\bar{\tau}) + \log_{10}(\eta), \quad (6)$$

Considering that η varies generally in a rather narrow range (i.e., from 0.02 to 0.08; McGarr, 1999), EI can be thought as a proxy for the mean loading stress during an event, and thus it can be regarded as useful for monitoring temporal variations in the dynamic properties of the earthquakes.

4. Energy Index Temporal and Spatial Variation

The seismicity rate changes associated to the 2009 L'Aquila seismic sequence have been thoroughly studied. Mignan (2012) proposed a model that can explain the main changes in the seismicity rate. Here, we select among the events belonging to cat-P those with Mw 1.8–3.5 and depth 6–15 km (i.e., 68 earthquakes).

Figure (3a) shows the temporal evolution of EI during the preparatory phase. In the final part of the quiescence period (i.e., between 11-02-2009 and 30-03-2009), we observe a sudden increase of EI in four events before the ML 4.1 foreshock (red square), which according to most of the authors (e.g., Sgan et al., 2014) marks the begin of the activation phase and could also have been triggered by cascading events. The ML 4.1 foreshock does not show anomalous EI, but it is followed by a high number of events with small EI.

Figure 3b shows the cumulative number of events in cat-P, where the last two phases of the preparation process are highlighted: the Accelerating Seismic Release (ASR) and the short-term Activation identified by Mignan (2012), with the latter starting on 29 March 2009 and culminating with the Mw 6.1 earthquakes on 6 April 2009. Figure 3c shows the cumulative of EI (hereinafter ΣEI) for the same time period. To provide an estimate of the uncertainty associated with ΣEI , we follow a bootstrap approach (Efron, 1979), repeating the computation of ΣEI with 1,000 random sampling realizations of the original data set with replacement.

The seismicity rate and ΣEI present an opposite trend. When the activation phase starts and the seismicity rate increases, ΣEI shows a significant decrease (Figure 3c). Since Calderoni et al. (2019) did not observe stress-drop differences between foreshocks and aftershocks, the rapid decrease in ΣEI support the idea that the activation phase of the mainshock interested a focal volume with higher dynamic strength.

Figure 3c provides also the distance of the foreshocks from the hypocenter of the mainshock. During the Activation, foreshocks occur within a region with distance of approximately 4–6 km from the mainshock, without evidence of further approach to the mainshock hypocenter. This spatial pattern for foreshocks is compatible with the observations from Ben-Zion and Zaliapin (2020) for the Parkfield earthquake, where the seismicity was observed to scatter before the mainshock, likely indicating the progressive increasing in stress levels around a main asperity responsible for failures over a progressively wider region.

However, we cannot exclude that earthquakes smaller than those examined in this work may show a different behavior. For example, Sgan et al. (2014) observed events with Mw < 1.8 approaching the hypocenter of the main event. Similar observations have also been reported in other region of normal-fault type earthquakes (e.g., Yao et al., 2020).

We follow Picozzi et al. (2021) to map EI in space. We create a regular three-dimensional grid of size 1 km. For each grid node, we select events within a maximum distance from the cell equal to one and half times the size of the grid node. Following Nandan et al. (2016), if the ratio of the distance between a grid node and a source (D) with respect to the source event length (L) is less than 10, we can assume that the static stress transfer becomes negligible. We compute L for all events considering the Brune's model (Brune, 1970) and assuming a constant stress-drop equal to 1 MPa. For each node, we keep only those events compliant with the above criteria ($D/L \leq 10$).

We compute the mean of EI for the selected events, EI , and we assign it to the considered node. Thus, EI provides information on the average characteristic of the population of events occurring in the proximity of each node. We map EI for the Activation phase (Figure 3d) and for the period from L'Aquila Mw 6.1 to the most important aftershock (i.e., the Campotosto Mw 5.4 earthquake, which occurred on 7 April 2009 at 19:47 UTC time, Figure 3e).

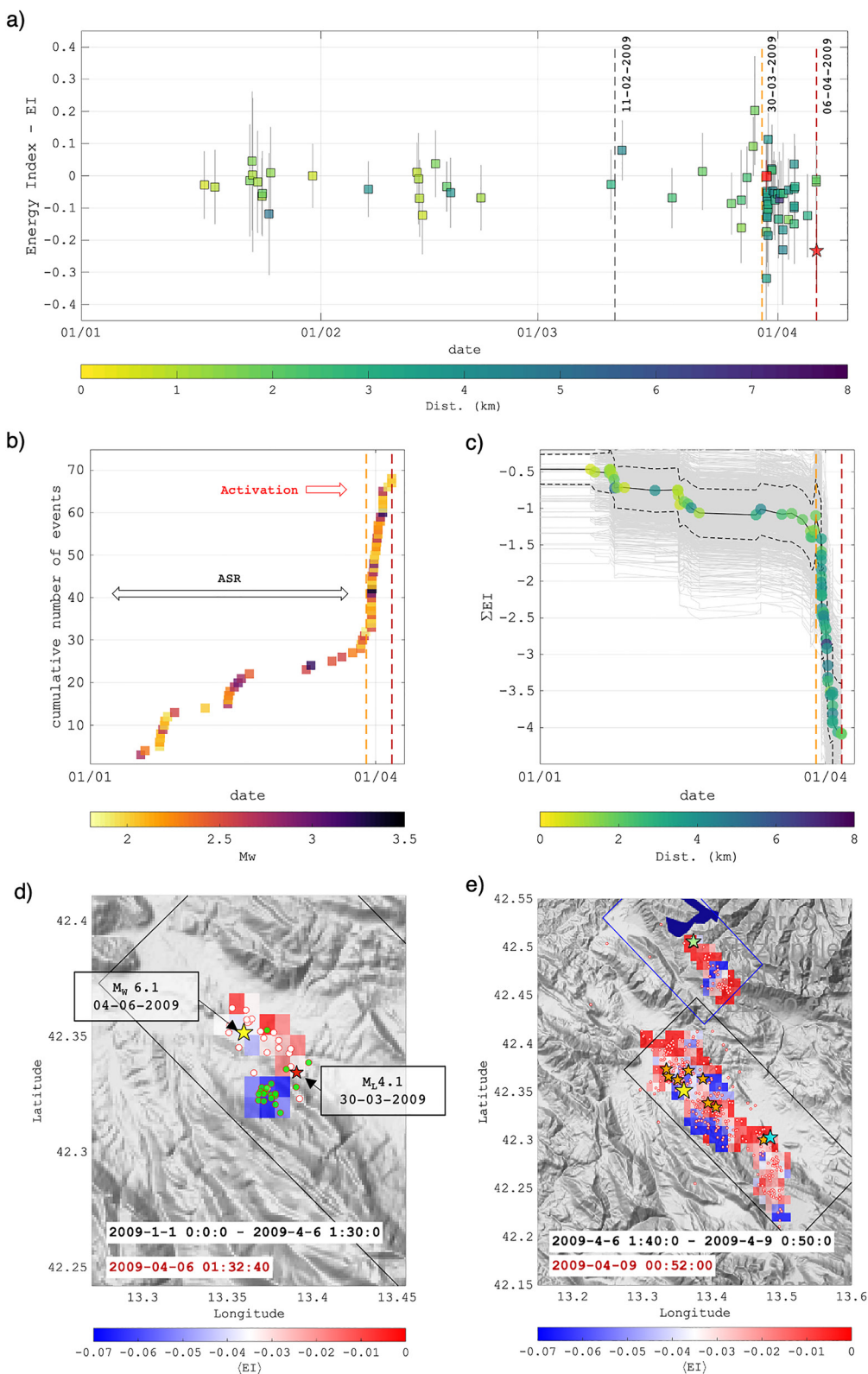


Figure 3.

In Figure 3d, we use a different color for foreshocks belonging to the preparatory phase before and after the activation onset (i.e., in white those occurring before 30 March 2009, and in green those in the activation phase). Figure 3d shows that all nodes have negative *EI* values, but also not uniform distribution. Foreshocks during the initial stage of the preparatory phase (white dots) have larger *EI* and are spread between the ML 4.1 foreshock and the mainshock. In contrast, foreshocks in the activation phase show lower *EI* values and appear concentrated in an area a few kilometers south of the main shock hypocenter.

Even after the mainshock, the *EI* distribution depicts a peculiar irregular pattern. Figure 3e shows the *EI* distribution for period between the Mw 6.1 L'Aquila mainshock and the Mw 5.4 Campotosto earthquake. The area surrounding the mainshock hypocenter and other areas located in the lower and upper portions of the fault are characterized by small *EI* values. In contrast, the largest *EI* values are observed in areas located both toward the northern edge and in the central part of the Paganica fault, where the Mw 5.2 aftershock on 9 April 2009 at 00:52 UTC occurred (cyan star in Figure 3e).

5. Discussion & Conclusion

This study was motivated by the growing need to find strategies for monitoring the evolution of seismic sequences and to identify the preparatory phase of large earthquakes. We explored this issue by focusing on a well-known case, namely the preparatory phase of the 2009 Mw 6.1 L'Aquila earthquake, and by studying the dynamic characteristics of small earthquakes occurred during the months preceding the mainshock.

The preparatory phase of L'Aquila earthquake has been studied in the last decade by various authors and from different perspectives. Among them, Sgan et al. (2014) applied a cross-correlation matched filter technique and extracted 3,571 foreshocks in the magnitude range $-0.4\text{--}3.9$. They identified three distinct phases in the preparatory of L'Aquila earthquake: (a) occurrence of seismic bursts north-west of the mainshock hypocenter until the mid-February, during which the seismicity migrated at a rate of $\sim 0.5 \text{ km/day}$ toward the Mw 6.1 hypocenter; (b) a cumulative increase in the number of earthquakes associated with a low b-value zone of about 4 km^2 located near the mainshock hypocenter, which lasted until the onset of the activation phase; (c) an activation phase characterized by a high rate of events with moderate to high b-value concentrated in an area south to the mainshock hypocenter.

We investigated the preparatory phase of L'Aquila earthquake by studying the temporal evolution and spatial distribution of M_0 and E_S . We introduced a new parameter defined *EI*, which represents the deviation of the scaling between M_0 and E_S for foreshocks from a model calibrated during a period characterized by background seismicity. Calderoni et al. (2019) studied the temporal evolution of the Savage and Wood efficiency, η_{SW} (Savage & Wood, 1971) and observed its decrease in the days immediately before and after the mainshock. With a larger number of smaller foreshocks, we were able to detect a marked decrease in the energy radiation of foreshocks during the activation phase, and to map their spatial distribution, which well corresponds to the area with highest b-value identified by Sgan et al., 2014.

The temporal evolution of *EI* complements the information provided by the seismic rate. Both parameters, in fact, highlight the onset of the activation phase, for which *EI* suggests that foreshocks were characterized by a progressive increase in slip per stress unit. These observations agree with the diffusion of highly pressurized fluids into the hanging wall volume before the L'Aquila earthquake, as proposed by Lucente et al. (2010). The spatial distribution of *EI* suggests heterogeneity of fault properties. The two larger aftershocks (i.e., the Mw 5.2 and Mw 5.4 Campotosto earthquakes) have both occurred in areas with larger *EI*.

Figure 3. (a) Temporal evolution of energy index (*EI*) (data colored per hypocentral distance from the L'Aquila earthquake) with standard error (vertical black lines). *EI* values for the 30-03-2009 ML 4.1 foreshock (red square) and the Mw 6.1 L'Aquila earthquake (red star). The time for the quiescence and activation phases (gray and red dashed lines, respectively) and the time of occurrence for the L'Aquila earthquake (red dashed line) is also plotted. (b) Cumulative number of events observed prior to the L'Aquila earthquake. Start of the activation phase (yellow dashed line) and time of occurrence for the L'Aquila earthquake (red dashed line). (c) Temporal evolution for the cumulative of *EI* (data colored per hypocentral distance from the L'Aquila earthquake). Temporal evolution of bootstrap replication of the original set of *EI* (gray lines), mean value (black line) and mean ± 1 standard deviation (black dashed lines). (d) Map showing for the L'Aquila earthquake preparatory phase the spatial distribution of the average of *EI* values associated to each grid node of the mesh considered in the investigated area. Epicenters of the L'Aquila earthquake (yellow star), ML 4.1 foreshock (red star), events with $Mw > 3.5$ (orange stars), foreshocks belonging to the ASR phase (white dots with red contour) and for the activation phase (green dots). The rectangles depict the surface projection of the Paganica (black line) and Campotosto (blue line) faults as given in Malagnini et al. (2012). (e) The same as (d), but for the period between L'Aquila earthquake and the Mw 5.4 Campotosto earthquake (light green star). The Mw 5.2 aftershock is represented as cyan star.

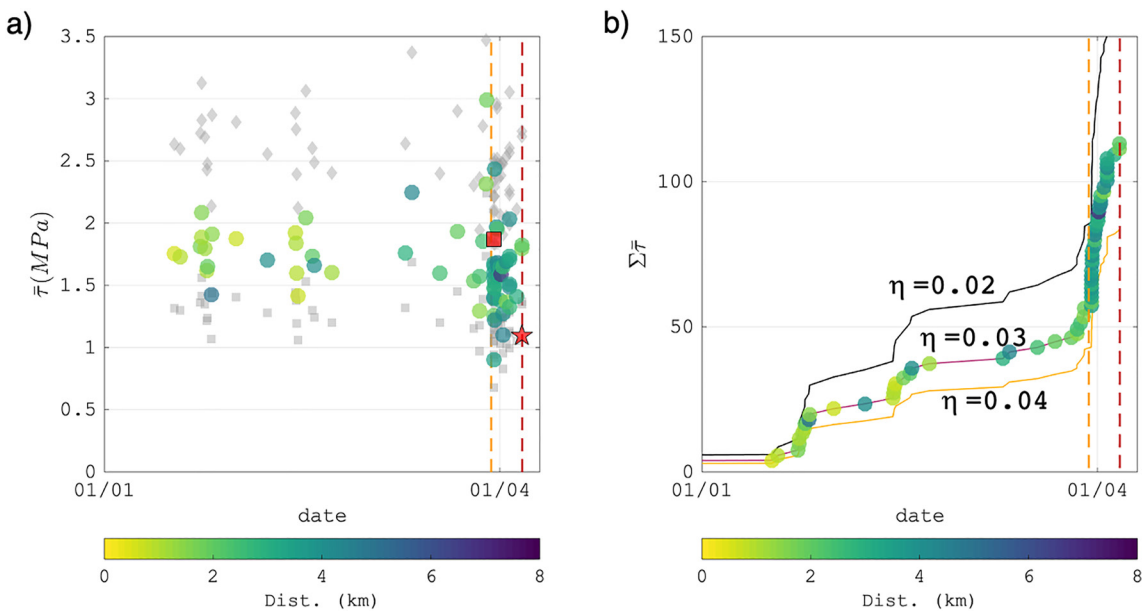


Figure 4. Temporal evolution of $\bar{\tau}$ estimates for $\eta = 0.03$ (data are colored per hypocentral distance from the L'Aquila hypocenter), for $\eta = 0.02$ (gray diamonds) and 0.04 (gray squares). Start of the activation phase (yellow dashed line) and time of occurrence for the L'Aquila earthquake (red dashed line). (b) Cumulative of $\bar{\tau}$ for $\eta = 0.03$ (data colored as in (a)) and for η varying from 0.02 (black line) to 0.04 (yellow line).

According to Equation 6, EI is related to the seismic efficiency, η , and the average loading stress, $\bar{\tau}$. McGarr (1999) observed that η generally varies in a rather narrow range (i.e., from 0.02 to 0.08) and suggested $\eta \leq 0.06$ for crustal earthquakes in California. Here, we reconsider the values of η and η_{SW} proposed by McGarr (1999) to fit a linear model (Figure S5a in Supporting Information S1) applied to estimate η corresponding to the values of η_{SW} provided by Calderoni et al., 2019 for the foreshocks (Figure S5b in Supporting Information S1). This allows us obtaining an estimate of the average η equal to 0.03 (± 0.01). Therefore, we combine Equation 5 and 6 and assume $\eta = 0.03$, to obtain a first order approximation of $\bar{\tau}$ and its variation during the ASR and Activation phases of the M_w 6.1 L'Aquila preparation process. Figure 4a shows that during the ASR phase, $\bar{\tau}$ varies between 1.5 and 2 MPa. Note that considering η equal to 0.02 or 0.04, the maximum and minimum $\bar{\tau}$ are of the order of 3 and 1 MPa, respectively. When the Activation phase starts, $\bar{\tau}$ shows a decrease with values mostly around 1.5 MPa and 1 below.

Because we selected only events with M_w between 1.8 and 3.5, our results support the idea that small earthquakes can provide important information about the dynamic processes acting during the preparation phase of large earthquakes.

Figure 4b shows the cumulative of $\bar{\tau}$ (i.e., $\Sigma\bar{\tau}$), which we computed to facilitate the comparison with the seismicity rate in Figure 3b. Please note that in Figure 4b we provide the cumulative of $\bar{\tau}$ estimates also for η equal to 0.02 and 0.04. We compare the rate of $\bar{\tau}$ increase in time for ASR and Activation (i.e., we consider $\eta = 0.03 \pm 0.01$). For ASR, we observe the shear stressing rate being 0.026 MPa/hr (ranging from 0.02 to 0.04 MPa/hr according to the selected variation of η), while for the activation it rises to 0.34 MPa/hr (ranging from 0.24 to 0.45 MPa/hr).

With this in mind, we can imagine that real-time EI estimations derived by approaches like RAMONES (Spaliarossa et al., 2021) can provide information during seismic monitoring that, combined with other parameters (e.g., seismicity rate, b-value, V_p/V_S), will help improving short-term hazard estimates. For instance, a procedure like the one by Giulia and Wiemer (2019) for the real-time discrimination of foreshocks and aftershocks could benefit from EI estimations.

It is worth also noting that estimating E_s for very small magnitude events is still an open issue, which represents in our opinion the main actual limitation of our approach. Indeed, having a threshold to M_w 1.8 for the estimation of E_s , we can characterize EI only for few tens of events during the most important period of the preparatory phase, while Sgan et al. (2014) have shown that catalogs of thousands of foreshocks could be, in principle, exploitable.

For this reason, further efforts should focus on strategies for the dynamic characterization of very small events. Despite such limitation, we believe that our results provide useful information on the preparatory process of the L'Aquila earthquake and demonstrate the potential of studying the dynamic characteristics of small magnitude earthquakes for studying the temporal evolution of seismic sequence and intercept hints of large earthquake preparatory processes.

Conflict of Interest

The authors declare no conflicts of interest relevant to this study.

Data Availability Statement

We used data and information retrieved from ORFEUS-EIDA (<https://www.orfeus-eu.org/data/eida/>), IRIS (<https://www.iris.edu/hq/>) and DPC (<http://ran.protezionecivile.it/EN/index.php>). We used data mainly from networks IV (<http://doi.org/10.13127/SD/X0FXnH7QfY>), IT (<https://doi.org/10.7914/SN/IT>) and MN (<https://doi.org/10.13127/SD/fBBBtDtd6q>).

Acknowledgments

We would like to thank the Editor G. Prieto, R. Castro and another anonymous reviewer for their comments and suggestions that allowed us to significantly improve the manuscript content and form. This research was partly carried out in the frame of Programme STAR PLUS (project DRAGON), financially supported by UniNA and Compagnia di San Paolo. Figures were done using Matlab software (R2019b, <https://it.mathworks.com/>, last accessed December 2021). Open Access Funding provided by Università degli Studi di Napoli Federico II within the CRUI-CARE Agreement.

References

- Abbott, A., & Nosengo, N. (2014). Italian seismologists cleared of manslaughter. *Nature*, 515, 171. <https://doi.org/10.1038/515171a>
- Ben-Zion, Y., & Zaliapin, I. (2020). Localization and coalescence of seismicity before large earthquakes. *Geophysical Journal International*, 223(1), 561–583. <https://doi.org/10.1093/gji/ggaa315>
- Bindi, D., Spallarossa, D., Picozzi, M., & Morasca, P. (2020). Reliability of source parameters for small events in central Italy: Insights from spectral decomposition analysis applied to both synthetic and real data. *Bulletin of the Seismological Society of America*, 110(6), 3139–3157. <https://doi.org/10.1785/0120200126>
- Bindi, D., Spallarossa, D., Picozzi, M., Scafidi, D., & Cotton, F. (2018). Impact of magnitude selection on aleatory variability associated with ground-motion prediction equations: Part I—ILocal, energy, and moment magnitude calibration and stress-drop variability in central Italy. *Bulletin of the Seismological Society of America*, 108(3A), 1427–1442. <https://doi.org/10.1785/0120170356>
- Bindi, D., Zaccarelli, R., Strollo, A., & Di Giacomo, D. (2019). Harmonized local magnitude attenuation function for Europe using the European Integrated Data Archive (EIDA). *Geophysical Journal International*, 218(1), 519–533. <https://doi.org/10.1093/gji/ggz178>
- Boncio, P., Pizzi, A., Brozzetti, F., Pomposo, G., Lavecchia, G., Di Nuccio, D., & Ferrarini, F. (2010). Coseismic ground deformation of the 6 April 2009 L'Aquila earthquake (central Italy, Mw6.3). *Geophysical Research Letters*, 37, L06308. <https://doi.org/10.1029/2010GL042807>
- Borghi, A., Aoudia, A., Javed, F., & Barzaghi, R. (2016). Precursory slow-slip loaded the 2009 L'Aquila earthquake sequence. *Geophysical Journal International*, 205(2), 776–784. <https://doi.org/10.1093/gji/ggw046>
- Bouchon, M., Durand, V., Marsan, D., Karabulut, H., & Schmittbuhl, J. (2013). The long precursory phase of most large interplate earthquakes. *Nature Geoscience*, 6, 299–302. <https://doi.org/10.1038/ngeo1770>
- Brown, L., & Hudyma, M. (2017). Identification of stress change within a rock mass through apparent stress of local seismic events. *Rock Mechanics and Rock Engineering*, 50(1), 81–88. <https://doi.org/10.1007/s00603-016-1092-z>
- Brune, J. N. (1970). Tectonic stress and the spectra of seismic shear waves from earthquakes. *Journal of Geophysical Research*, 75(26), 4997–5009. <https://doi.org/10.1029/jb075i026p04997>
- Calderoni, G., Rovelli, A., & Di Giovambattista, R. (2019). Stress drop, apparent stress, and radiation efficiency of clustered earthquakes in the nucleation volume of the 6 April 2009, Mw 6.1 L'Aquila earthquake. *Journal of Geophysical Research: Solid Earth*, 124, 360–375. <https://doi.org/10.1029/2019jb017513>
- Chen, X. W., & Shearer, P. M. (2013). California foreshock sequences suggest aseismic triggering process. *Geophysical Research Letters*, 40, 2602–2607. <https://doi.org/10.1002/grl.50444>
- Chiareluce, L., Valoroso, L., Piccinini, D., Di Stefano, R., & De Gori, P. (2011). The anatomy of the 2009 L'Aquila normal fault system (central Italy) imaged by high resolution foreshock and aftershock locations. *Journal of Geophysical Research*, 116, B12311. <https://doi.org/10.1029/2011JB008352>
- De Gori, P., Lucente, F. P., Lombardi, A. M., Chiarrappa, C., & Montuori, C. (2012). Heterogeneities along the 2009 L'Aquila normal fault inferred by the b-value distribution. *Geophysical Research Letters*, 39, L15304. <https://doi.org/10.1029/2012GL052822>
- Di Luccio, F., Ventura, G., Di Giovambattista, R., Piscini, A., & Cinti, F. R. (2010). Normal faults and thrusts reactivated by deep fluids: The 6 April 2009 Mw 6.3 L'Aquila earthquake, central Italy. *Journal of Geophysical Research*, 115, B06315. <https://doi.org/10.1029/2009JB007190>
- Dresen, G., Kwiatak, G., Goebel, T., & Ben-Zion, Y. (2020). Seismic and aseismic preparatory processes before large stick-slip failure. *Pure and Applied Geophysics*, 177, 5741–5760. <https://doi.org/10.1007/s00024-020-02605-x>
- Efron, B. (1979). Bootstrap methods: Another look at the jackknife. *Annals of Statistics*, 7, 1–26. <https://doi.org/10.1214/aos/1176344552>
- Gulia, L., & Wiemer, S. (2019). Real-time discrimination of earthquake foreshocks and aftershocks. *Nature*, 574, 193–199. <https://doi.org/10.1038/s41586-019-1606-4>
- Herrmann, R. B., Malagnini, L., & Munafò, I. (2011). Regional moment tensors of the 2009 L'Aquila earthquake sequence. *Bulletin of the Seismological Society of America*, 101, 975–993. <https://doi.org/10.1785/0120100184>
- Kanamori, H., & Heaton, T. H. (2000). Microscopic and macroscopic Physics of earthquakes. In J. B. Rundle, D. L. Turcotte, & W. Klein (Eds.), *Geocomplexity and the Physics of earthquakes* (pp. 147–163). <https://doi.org/10.1029/GM120p0147>
- Kato, A., & Ben-Zion, Y. (2020). The generation of large earthquakes. *Nature Reviews Earth & Environment*, 2(1), 26–39. <https://doi.org/10.1038/s43017-020-00108-w>
- Kato, A., Obara, K., Igarashi, T., Tsuruoka, H., Nakagawa, S., & Hirata, N. (2012). Propagation of slow slip leading up to the 2011 Mw 9.0 Tohoku-Oki earthquake. *Science*, 335, 705–708. <https://doi.org/10.1126/science.1215141>

- Lucente, F. P., De Gori, P., Piccini, D., Di Bona, M., Chiarabba, C., & Piana Agostinetti, N. (2010). *Temporal variation of seismic velocity and anisotropy before the 2009 Mw 6.3 L'Aquila earthquake, Italy*. *Geology*, 38(11), 1015–1018. <https://doi.org/10.1130/G31463.1>
- Malagnini, L., Lucente, F. P., De Gori, P., Akinci, A., & Munafò, I. (2012). Control of pore fluid pressure diffusion on fault failure mode: Insights from the 2009 L'Aquila seismic sequence. *Journal of Geophysical Research*, 117, B05302. <https://doi.org/10.1029/2011JB008911>
- Malin, P. E., Bohnhoff, M., Blümle, F., Dresen, G., Martínez-Garzón, P., Nurlu, M., et al. (2018). Microearthquakes preceding a M4.2 earthquake offshore Istanbul. *Scientific Reports*, 8, 16176. <https://doi.org/10.1038/s41598-018-34563-9>
- McGarr, A. (1999). On relating apparent stress to the stress causing earth-quake fault slip. *Journal of Geophysical Research*, 104(B2), 3003–3011. <https://doi.org/10.1029/1998jb900083>
- Mignan, A. (2012). Seismicity precursors to large earth- quakes unified in a stress accumulation framework. *Geophysical Research Letters*, 39, L21308. <https://doi.org/10.1029/2012GL053946>
- Nandan, S., Oullion, G., Woessner, J., Sornette, D., & Wiemer, S. (2016). Systematic assessment of the static stress triggering hypothesis using interearthquake time statistics. *Journal of Geophysical Research: Solid Earth*, 121, 1890–1909. <https://doi.org/10.1002/2015JB012212>
- Picozzi, M., Bindì, D., Brondi, P., Di Giacomo, D., Parolai, S., & Zollo, A. (2017). Rapid determination of P wave- based energy magnitude: Insights on source parameter scaling of the 2016 central Italy earthquake sequence. *Geophysical Research Letters*, 44, 4036–4045. <https://doi.org/10.1002/2017gl073228>
- Picozzi, M., Bindì, D., Festa, G., Cotton, F., Scala, A., & D'Agostino, N. (2021). Spatio-temporal evolution of microseismicity seismic source properties at the Irpinia near fault observatory, Southern Italy. *Bulletin of the Seismological Society of America*, 112(1), 226–242. <https://doi.org/10.1785/0120210064>
- Picozzi, M., Bindì, D., Spallarossa, D., Di Giacomo, D., & Zollo, A. (2018). A rapid response magnitude scale for timely assessment of the high frequency seismic radiation. *Scientific Reports – Nature*, 8, 8562. <https://doi.org/10.1038/s41598-018-26938-9>
- Picozzi, M., Bindì, D., Spallarossa, D., Oth, A., Di Giacomo, A., Zollo, A., et al. (2019). Moment and energy magnitudes: Diversity of views on earthquake shaking potential and earthquake statistics. *Geophysical Journal International*, 216, 1245–1259. <https://doi.org/10.1093/gji/ggy488>
- Picozzi, M., Bindì, D., Zollo, A., Festa, G., & Spallarossa, D. (2019). Detecting long-lasting transients of earthquake activity on a fault system by monitoring apparent stress, ground motion and clustering. *Scientific Reports*, 9, 16268. <https://doi.org/10.1038/s41598-019-52756-8>
- Savage, J. C., & Wood, M. D. (1971). The relation between apparent stress and stress drop. *Bulletin of the Seismological Society of America*, 61, 1381–1388. <https://doi.org/10.1785/bssa0610041009>
- Scafidi, D., Spallarossa, D., Ferretti, G., Barani, S., Castello, B., & Margheriti, L. (2019). A complete automatic procedure to compile reliable seismic catalogs and travel-time and strong-motion parameters datasets seism. *Seismological Research Letters*, 90(3), 1308–1317. <https://doi.org/10.1785/0220180257>
- Schurr, B., Asch, G., Hainzl, S., Bedford, J., Hoechner, A., Palo, M., et al. (2014). Unlocking of plate boundary controlled initiation of the 2014 Iquique earthquake. *Nature*, 512, 13681. <https://doi.org/10.1038/nature13681>
- Socquet, A., Piñá-Valdés, J., Jara, J., Cotton, F., Walpersdorf, A., Cotte, N., et al. (2017). An 8 month slow slip event triggers progressive nucleation of the 2014 Chile megathrust. *Geophysical Research Letters*, 44, 4046–4053. <https://doi.org/10.1002/2017gl073023>
- Spallarossa, D., Ferretti, G., Scafidi, D., Turino, C., & Pasta, M. (2014). Performance of the RSNI-Picker. *Seismological Research Letters*, 85(6), 1243–1254. <https://doi.org/10.1785/0220130136>
- Spallarossa, D., Picozzi, M., Scafidi, D., Morasca, P., Turino, C., & Bindì, D. (2021). The RAMONES service for rapid assessment of seismic moment and radiated energy in central Italy: Concepts, capabilities, and future perspectives. *Seismological Research Letters*, 92(3), 1759–1772. <https://doi.org/10.1785/0220200348>
- Sugan, M., Kato, A., Miyake, H., Nakagawa, S., & Vuan, A. (2014). The preparatory phase of the 2009 Mw 6.3 L'Aquila earthquake by improving the detection capability of low-magnitude foreshocks. *Geophysical Research Letters*, 41, 6137–6144. <https://doi.org/10.1002/2014gl061199>
- Terakawa, T., Zoporowski, A., Galvan, B., & Miller, S. A. (2010). High-pressure fluid at hypocentral depths in the L'Aquila region inferred from earthquake focal mechanisms. *Geology*, 38, 995–998. <https://doi.org/10.1130/G31457.1>
- Valoroso, L., Chiaraluce, L., Piccinini, D., Di Stefano, R., Schaff, D., & Waldhauser, F. (2013). Radiography of a normal fault system by 64,000 high-precision earthquake locations: The 2009 L'Aquila (central Italy) case study. *Journal of Geophysical Research: Solid Earth*, 118, 1156–1176. <https://doi.org/10.1002/jgrb.50130>
- Wyss, M., & Brune, J. N. (1968). Seismic moment, stress, and source dimensions for earthquakes in the California-Nevada region. *Journal of Geophysical Research*, 73, 4681–4694. <https://doi.org/10.1029/jb073i014p04681>
- Yao, D., Huang, Y., Peng, Z., & Castro, R. R. (2020). Detailed investigation of the foreshock sequence of the 2010 Mw7.2 El Mayor-Cucapah earthquake. *Journal of Geophysical Research: Solid Earth*, 124, e2019JB019076. <https://doi.org/10.1029/e2019JB019076>
- Yoon, C. E., Yoshimitsu, N., Ellsworth, W. L., & Beroza, G. C. (2019). Foreshocks and mainshock nucleation of the 1999 Mw 7.1 Hector Mine, California, earthquake. *Journal of Geophysical Research: Solid Earth*, 124, 1569–1582. <https://doi.org/10.1029/2018JB016383>